15. In separate experiments, EOF-generating fields of up to 700 V/cm have been applied to transparent insulated microchannels without flowFETs. Gate voltages of 100 V (equal to fields as large as 2.6 MV/cm) have been applied to channel walls before electrical breakthrough occurred.
16. In accordance with the tradition of reporting gate voltages in metal-oxide semiconductor FETs, the potential difference between the gate contact and the end of the channel is reported. The actual potential difference between the gate contacts and the fluid opposite them differs from the reported voltages by an amount equal to the potential drop in the channel between the flowFET gate and the end of the channel. This depends on the exact channel geometry and is estimated to be around 12.5 V.
17. A. van den Berg, Netherlands Patent NL-1010327, priority date 15 October 1998.

2 June 1999; accepted 24 September 1999

Organic-Inorganic Hybrid Materials as Semiconducting Channels in Thin-Film Field-Effect Transistors

C. R. Kagan, D. B. Mitzi, C. D. Dimitrakopoulos

Organic-inorganic hybrid materials promise both the superior carrier mobility of inorganic semiconductors and the processability of organic materials. A thin-film field-effect transistor having an organic-inorganic hybrid material as the semiconducting channel was demonstrated. Hybrids based on the perovskite structure crystallize from solution to form oriented molecular-scale composites of alternating organic and inorganic sheets. Spin-coated thin films of the semiconducting perovskite $(C_6H_5C_2H_4NH_3)_2SnI_4$ form the conducting channel, with field-effect mobilities of 0.6 square centimeters per volt-second and current modulation greater than 10^4. Molecular engineering of the organic and inorganic components of the hybrids is expected to further improve device performance for low-cost thin-film transistors.

Alternative semiconducting materials for thin-film field-effect transistors (TFTs), which have mobilities at least comparable to that of amorphous silicon (a-Si) and may also be easily processed with low-cost techniques, are required to enable new opportunities for display and storage technologies. Conjugated organic small molecules (*1–4*), short-chain oligomers (*5, 6*), and long-chain polymers (*7–10*) continue to receive substantial attention as new semiconducting channels for TFTs. Organic semiconductors may be deposited by low-cost, low-temperature processes such as spin coating, dip coating, or screen printing from solution or thermal evaporation. These techniques provide a potential niche for organic semiconductors in applications that require large areas, low cost, mechanical flexibility, or a combination of these factors. Examples of applications include TFTs for active matrix liquid crystal displays (AMLCDs), where a-Si is presently used; active matrix organic light-emitting diodes (AMOLEDs); and low-cost data storage devices. In addition, low-temperature deposition conditions enable organic semiconductors to be deposited on plastic substrates for flexible electronic devices (*11, 12*).

In organic semiconductors, π-orbital overlap between adjacent conjugated molecules enables charge transport, but the weak van der Waals interaction bonding neighboring molecules limits their carrier mobilities. The highest mobilities reported for organic TFTs have been achieved by vacuum evaporation of ordered thin films of either small molecules (*3*) or short-chain oligomers (*6*). Molecular ordering improves orbital overlap and therefore film mobility. Although evaporated films demonstrate mobilities comparable to that of a-Si (0.1 to 1 $cm^2/V \cdot s$), the high vacuum used makes deposition costly. Solution-based deposition techniques, such as spin coating, are the most desirable processes because they are both cheap and large-area deposition methods. Long-chain polymers are soluble enough to be spin coated, but their mobilities, 10^{-8} to 10^{-2} $cm^2/V \cdot s$, are lower because films are more disordered (*9*). Recently a soluble pentacene precursor was synthesized and converted to yield mobilities of 0.1 $cm^2/V \cdot s$ (*4*). The low carrier mobilities of organic TFTs limit their device-switching speeds and therefore their range of potential applications.

Organic-inorganic hybrid materials combine the advantageous properties characteristic of crystalline inorganic solids with those of organic molecules within a molecular-scale composite. The inorganic component forms an extended framework bound by strong covalent or ionic (or both) interactions to provide high carrier mobilities. The organic component facilitates the self-assembly of these materials, enabling hybrids to be deposited by the same simple, low-cost, low-temperature processes as the organic materials. The organic component is also used to tailor the electronic properties of the inorganic framework by defining its reduced dimensionality and by mediating the electronic coupling between inorganic units. Engineering the organic-inorganic hybrid on the molecular scale may be done to maximize both field-effect mobility and current modulation. The combination of high carrier mobility and ease of processing may make organic-inorganic hybrid materials good substitutes in all the applications put forth for organic materials. The potentially higher carrier mobilities of hybrid materials may extend their application to higher speed devices than is presently possible with either a-Si or organic semiconductors.

One class of organic-inorganic hybrid is based on the three-dimensional (3D) perovskite structure ABX_3 (Fig. 1). The chemistry of the organic and inorganic components of the perovskite can be tailored to tune the electronic, optical, magnetic, and mechanical properties of hybrid materials (*13*). Although most organic-inorganic perovskites are insulating, hybrids having a tin(II) iodide framework are electrically conductive. Hall measurements on pressed pellet samples of the 3D perovskite $CH_3NH_3SnI_3$ reveal that it is a low-carrier-density metal with a room temperature Hall mobility of 50 $cm^2/V \cdot s$ (*14*). Layered perovskites of the form $A_2A'_{n-1}Sn_nI_{3n+1}$ may also be prepared by stacking n inorganic layers, containing a small A′ cation, separated by organic layers of a larger A cation. Systematic study of the effects of dimensionality has shown a metal-to-semiconductor transition as n is reduced from $n \rightarrow \infty$ for the 3D hybrid to $n = 1$, for the 2D layered hybrid (*15*). Although the conductivity is reduced with decreasing dimensionality, high carrier mobilities are expected for the layered perovskites because they consist of the same extended inorganic framework of corner-sharing SnI_6 octahedra that gives rise to the high carrier mobility of the 3D analog $CH_3NH_3SnI_3$.

We demonstrated an organic-inorganic TFT using the 2D layered organic-inorganic perovskite $(C_6H_5C_2H_4NH_3)_2SnI_4$ as the semiconducting channel. $(C_6H_5C_2H_4NH_3)_2SnI_4$ is synthesized by dissolving stoichiometric quantities of SnI_2 and the organic salt, $C_6H_5C_2H_4NH_2 \cdot HI$ in concentrated (57 weight %) aqueous HI at 90°C under flowing N_2. Crystals of the compound $(C_6H_5C_2H_4NH_3)_2SnI_4$ precipitate from solution upon cooling to room temperature. The crystals are filtered, rinsed in 5:1 toluene:*n*-butanol, and dried under vacuum. The crystals are redissolved at 20 mg/ml in anhydrous methanol. Solutions are filtered through a 0.2-μm polytetrafluoroethylene filter and spun onto wafers at 2500 rpm for 2 min in an inert atmo-

IBM T. J. Watson Research Center, Post Office Box 218, Yorktown Heights, NY, 10598, USA.

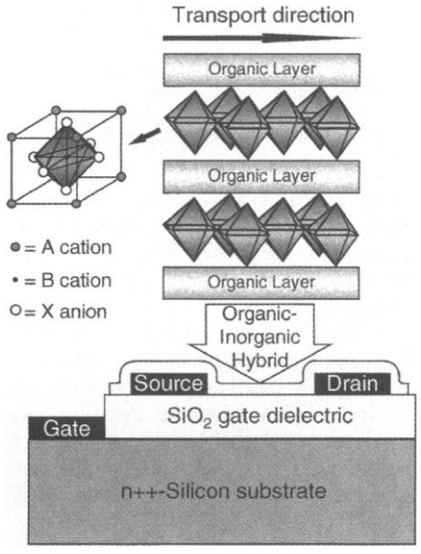

Fig. 1. Schematic of a TFT device structure having a layered organic-inorganic perovskite as the semiconducting channel. The perovskite structure ABX_3 comprises corner-sharing BX_6 octahedra. Each octahedron is defined by six X anions at the vertices and one B cation at the center. The A cations sit in the interstitial sites between octahedra. In the organic-inorganic perovskite, anionic, inorganic BX_4^{2-} sheets are charge-balanced by cationic organic molecules substituted in the A cation sites. The layered organic-inorganic perovskite can be visualized by inserting an organic layer between perovskite sheets.

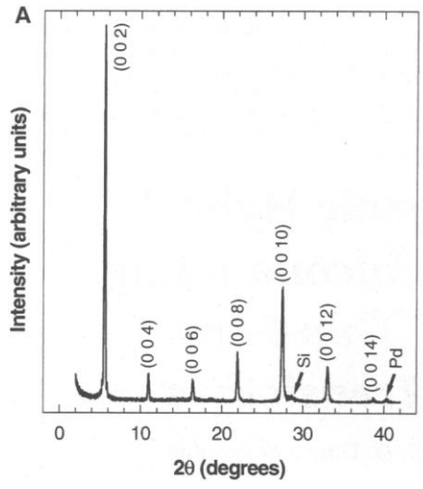

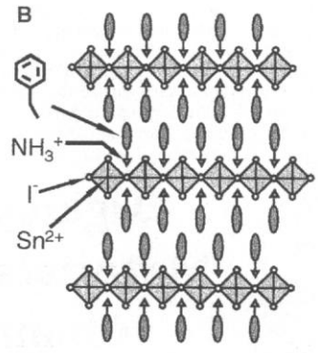

Fig. 2. (**A**) X-ray diffraction pattern for a completed TFT with $(C_6H_5C_2H_4NH_3)_2SnI_4$ as the semiconducting channel and Pd source and drain electrodes. (**B**) Representation of the organic-inorganic perovskite used in the device.

sphere. Thin films, ~300 Å thick, are dried and annealed at 80°C for 10 min. In the schematic device structure (Fig. 1), with a spin-coated organic-inorganic hybrid material used as the semiconducting channel, heavily *n*-doped silicon wafers with an indium contact are used as the gate electrode. The gate dielectric layer is a 400 Å, 1500 Å, or 5000 Å thermally grown oxide. High–work-function metal source and drain electrodes such as Pd, Pt, or Au are deposited by evaporation through a shadow mask either before or after spin coating. However, depositing the hybrid after metallization eliminates the material's exposure to potentially harmful temperatures. Devices were tested in a nitrogen box with a Hewlett-Packard 4145B semiconductor analyzer.

The organic-inorganic perovskites with metal halide frameworks are simple to deposit by methods such as spin coating (*16*), dip coating (*17*), or vacuum evaporation (*18, 19*). The layered organic-inorganic perovskites self-assemble from solution to form oriented polycrystalline films on substrates (Fig. 2). Ionic and covalent interactions between the metal cations and the halogen anions drive formation of an extended framework of inorganic SnI_6 octahedra. The organic, cationic, ammonium head groups form hydrogen and ionic bonds to halogens of the anionic metal halide octahedra to charge-balance the structure. Van der Waals interactions between organic tail groups on organic-inorganic-organic layers induce stacking of the layers to form the alternating, organic-inorganic, layered perovskite structure. The strong bonding between cationic and anionic species in the hybrid, not found in organic materials, requires the compound to have a specific stoichiometry and drives the organization of the organic and inorganic components into well-defined crystallographic sites.

In the x-ray diffraction pattern from a $(C_6H_5C_2H_4NH_3)_2SnI_4$ spin-coated device structure with Pd electrodes (Fig. 2), observation of only (0 0 ℓ) reflections from the organic-inorganic perovskite shows that the alternating organic-inorganic-organic layers stack perpendicular to the substrate surface. The (0 0 ℓ) reflections correspond to an interlayer distance of 16.3 Å separating the inorganic sheets (*20*). This geometry is ideal because the inorganic charge-carrying sheets extend in the direction of carrier transport. The progression of strong, sharp x-ray reflections is a measure of the high crystallinity and large grain size in spin-coated thin films. Scanning electron micrographs show that spin coating deposits uniform polycrystalline films with grain sizes exceeding 300 nm for thin films ~300 Å in thickness over the typically deposited ~1-cm^2 area.

A representative plot of drain current, I_D, versus source-drain voltage, V_{DS}, is shown as a function of the applied gate voltage V_G (Fig. 3A) for a TFT with $(C_6H_5C_2H_4NH_3)_2SnI_4$ as the semiconducting channel and a 5000 Å gate oxide. The layered organic-inorganic perovskite forms a *p*-channel transistor. The TFT operates in accumulation mode upon application of a negative bias to the gate electrode as the concentration of majority carriers contributing to I_D increases. Application of a positive

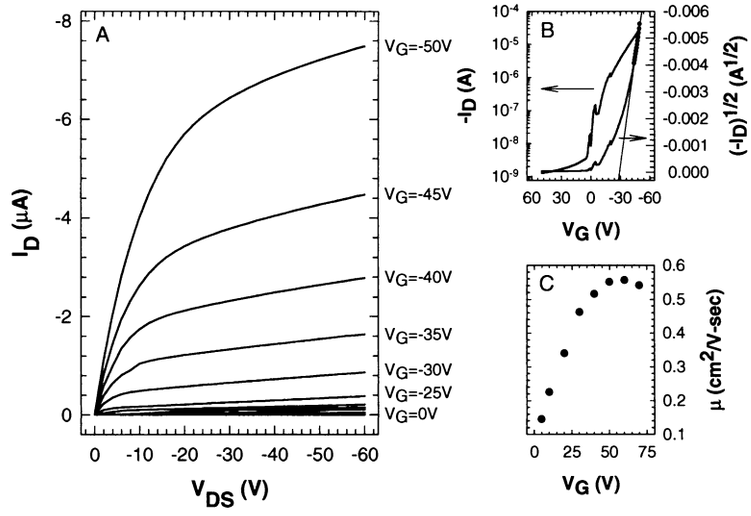

Fig. 3. (**A**) Drain current I_D versus source-drain voltage V_{DS} as a function of gate voltage V_G for a spin-coated $(C_6H_5C_2H_4NH_3)_2SnI_4$ thin-film transistor having a channel length L = 28 μm and channel width W = 1000 μm, defined by Pd source and drain electrodes. The gate dielectric is 5000 Å SiO_2. (**B**) Plots of I_D and $I_D^{1/2}$ versus V_G at constant V_{DS} = −100 V used to calculate current modulation and field-effect mobility, μ. (**C**) Plot of μ versus V_G at V_{DS} = −100 V.

gate bias depletes the channel of holes, turning the device off. At low V_{DS}, the TFT shows typical transistor behavior as I_D increases linearly with V_{DS}. Current saturation, with only a small ohmic component, is observed at high V_{DS} as the accumulation of holes in the channel is pinched off near the drain electrode.

Device operation is adequately modeled by the standard field-effect transistor equations that apply to both organic and inorganic TFTs. From the plot of I_D and $I_D^{1/2}$ versus V_G (Fig. 3B) used to calculate current modulation (I_{ON}/I_{OFF}) and field-effect mobility, μ, in the saturation regime, the field-effect mobility for this device is 0.55 $cm^2/V \cdot s$ for a $\pm$50-V sweep of V_G at $V_{DS} \geq 60$ V. This mobility is typical for $(C_6H_5C_2H_4NH_3)_2SnI_4$ as it has been calculated for many devices on the same wafer, on different wafers, and from different preparations of the hybrid. These same device characteristics scale to smaller voltages as the gate oxide thickness is reduced. The highest mobility measured for this material, on a 1500 Å gate oxide at $V_{DS} = -30$ V, is 0.62 $cm^2/V \cdot s$, which is six times higher than that of any other spin-coated material (*4*) and comparable to a-Si and the best organic semiconductors deposited in high vacuum.

The field-effect mobility of these organic-inorganic TFTs depends on V_G (Fig. 3C) as reported for organic TFTs (*12*) and a-Si (*21*). Increasing V_G increases the number of accumulated charges available in the channel to fill localized traps in the material. At higher V_G, the trap states are filled, enabling additional charges to move with carrier mobilities defined by the delocalized bands of the hybrid semiconductor. Filling of trap states is likely responsible for the discontinuities shown in Fig. 3B, which suggests that higher mobilities may be achieved at lower V_G in TFTs with high dielectric gate insulators, which may be deposited on plastic substrates (*12*).

Materials that can be solution processed and exhibit a high I_{ON}/I_{OFF} are required for TFTs in low-cost large-area applications. The $(C_6H_5C_2H_4NH_3)_2SnI_4$ TFT (Fig. 3B) has an I_{ON}/I_{OFF} of $>10^4$. There is an increase in leakage as V_{DS} increases for large positive V_G, limiting the current modulation. These on-off ratios are achieved without patterning the semiconductor to the active region between source and drain electrodes. The hybrid is spun across a ~1-cm^2 area of the wafer covering 16 devices. Patterning the semiconductor to the active device region reduces leakage through the insulator contributing to I_{OFF}, increasing I_{ON}/I_{OFF} to at least 10^6. Leakage, dominated by nonintentional dopants in unpatterned regions of the semiconductor away from the device, may be reduced by decreasing film thickness (*22*).

Organic-inorganic hybrid materials show the highest field-effect mobilities and I_{ON}/I_{OFF} ratios for spin-coated TFT channel materials. The cheap, low-temperature processing techniques suggest that organic-inorganic TFTs may be suitable for applications that require low cost, a large area, and the mechanical flexibility of plastic substrates. Semiconducting organic-inorganic hybrid materials may be designed with a wide range of organic and inorganic components for use in TFTs. Although $(C_6H_5C_2H_4NH_3)_2SnI_4$ has shown the best device characteristics, organic-inorganic perovskites with a tin(II) iodide framework and a variety of aliphatic (for example, alkyl-) and aromatic, ammonium, and diammonium cations have been incorporated in TFT devices and exhibit similar characteristics to those shown here. Increasing the dimensionality of the hybrid by increasing the number of repeated inorganic layers per organic layer may further increase film mobility. Improvements in materials processing and tailoring of the organic component are expected to increase mobilities in organic-inorganic TFTs with a SnI_2 framework up to at least 50 $cm^2/V \cdot s$. The flexibility in the chemistry of organic-inorganic hybrid materials may provide a path to preparation of both *n*-type and *p*-type transporting materials, which are necessary for complementary logic and normally "on" or "off" organic-inorganic TFTs.

References and Notes

1. A. R. Brown, A. Pomp, C. M. Hart, D. M. de Leeuw, *Science* **270**, 972 (1995).
2. C. D. Dimitrakopoulos, A. R. Brown, A. Pomp, *J. Appl. Phys.* **80**, 2501 (1996).
3. S. F. Nelson, Y. Y. Lin, D. J. Gundlach, T. N. Jackson, *Appl. Phys. Lett.* **72**, 1854 (1998).
4. P. T. Herwig, K. Müllen, *Adv. Mater.* **11**, 480 (1999).
5. G. Horowitz, D. Fichou, X. Peng, Z. Xu, F. Garnier, *Solid State Commun.* **72**, 381 (1989).
6. C. D. Dimitrakopoulos, B. Furman, T. Graham, S. Hegde, S. Purushothaman, *Synth. Met.* **92**, 47 (1998).
7. J. H. Burroughes, C. A. Jones, R. H. Friend, *Nature* **335**, 137 (1988).
8. A. Tsumura, H. Koezuka, T. Ando, *Appl. Phys. Lett.* **49**, 1210 (1986).
9. Z. Bao, A. Dodabalapur, A. J. Lovinger, *Appl. Phys. Lett.* **69**, 4108 (1996).
10. A. R. Brown, C. P. Jarrett, D. M. de Leeuw, M. Matters, *Synth. Met.* **88**, 37 (1997).
11. F. Garnier, R. Hajlaoui, A. Yassar, P. Srivastava, *Science* **265**, 1684 (1994).
12. C. D. Dimitrakopoulos, S. Purushothaman, J. Kymissis, A. Callegari, J. M. Shaw, *Science* **283**, 822 (1999).
13. For a review, see D. B. Mitzi, *Prog. Inorg. Chem.* **48**, 1 (1999).
14. D. B. Mitzi, C. A. Feild, Z. Schlesinger, R. B. Laibowitz, *J. Solid State Chem.* **114**, 159 (1995).
15. D. B. Mitzi, C. A. Feild, W. T. A. Harrison, A. M. Guloy, *Nature* **369**, 467 (1994).
16. C. Q. Xu *et al.*, *Solid State Commun.* **79**, 249 (1991).
17. K. Liang, D. B. Mitzi, M. T. Prikas, *Chem. Mater.* **10**, 304 (1998).
18. M. Era, T. Hattori, T. Taira, T. Tsutsui, *Chem. Mater.* **9**, 8 (1997).
19. D. B. Mitzi, M. T. Prikas, K. Chondroudis, *Chem. Mater.* **11**, 542 (1999).
20. G. C. Papavassiliou, I. B. Koutselas, A. Terzis, M. H. Whangbo, *Solid State Commun.* **91**, 695 (1994).
21. M. Shur, M. Hack, J. G. Shaw, *J. Appl. Phys.* **66**, 3371 (1989).
22. A. Dodabalapur, L. Torsi, H. E. Katz, *Science* **268**, 270 (1995).

23. We thank K. Chondroudis, J. Kymissis, and M. Prikas for technical assistance.

12 July 1999; accepted 23 September 1999

The Root of Angiosperm Phylogeny Inferred from Duplicate Phytochrome Genes

Sarah Mathews* and Michael J. Donoghue

An analysis of duplicate phytochrome genes (*PHYA* and *PHYC*) is used to root the angiosperms, thereby avoiding the inclusion of highly diverged outgroup sequences. The results unambiguously place the root near *Amborella* (one species, New Caledonia) and resolve water lilies (Nymphaeales, ~70 species, cosmopolitan), followed by *Austrobaileya* (one species, Australia), as early branches. These findings bear directly on the interpretation of morphological evolution and diversification within angiosperms.

The evolution of flowering plants fundamentally altered the biosphere. Deciphering the causes and consequences of their origin and radiation requires knowledge of phylogeny, especially the order in which branches diverged near the root of the tree (*1*). However, the root of angiosperms has remained unresolved, as different lines of evidence have suggested many disparate alternatives (*2*). This ambiguity stems in part from uncertainty surrounding the identity of their closest relatives (*3–5*), and from the great differences between angiosperms and all other living lines of seed plants. Such differences render homology assessments exceptionally difficult in morphological analyses, and may lead to "long branch attraction" in molecular analyses, which occurs when convergent nucleotide substitutions cause the spurious connection of highly diverged sequences (*6*). In analyses of angiosperms, distant outgroup sequences might connect (perhaps with confidence) to the most divergent angiosperm sequence or sequences. For this reason it has been suggested that the angiosperm root may never be resolved using nucleotide sequence

References and Notes

[1] **Logic Gates Made from Polymer Transistors and Their Use in Ring Oscillators**

A. R. Brown; A. Pomp; C. M. Hart; D. M. de Leeuw

Science, New Series, Vol. 270, No. 5238. (Nov. 10, 1995), pp. 972-974.

Stable URL:

http://links.jstor.org/sici?sici=0036-8075%2819951110%293%3A270%3A5238%3C972%3ALGMFPT%3E2.0.CO%3B2-8

[11] **All-Polymer Field-Effect Transistor Realized by Printing Techniques**

Francis Garnier; Ryad Hajlaoui; Abderrahim Yassar; Pratima Srivastava

Science, New Series, Vol. 265, No. 5179. (Sep. 16, 1994), pp. 1684-1686.

Stable URL:

http://links.jstor.org/sici?sici=0036-8075%2819940916%293%3A265%3A5179%3C1684%3AAFTRBP%3E2.0.CO%3B2-C

[12] **Low-Voltage Organic Transistors on Plastic Comprising High-Dielectric Constant Gate Insulators**

C. D. Dimitrakopoulos; S. Purushothaman; J. Kymissis; A. Callegari; J. M. Shaw

Science, New Series, Vol. 283, No. 5403. (Feb. 5, 1999), pp. 822-824.

Stable URL:

http://links.jstor.org/sici?sici=0036-8075%2819990205%293%3A283%3A5403%3C822%3ALOTOPC%3E2.0.CO%3B2-S

[22] **Organic Transistors: Two-Dimensional Transport and Improved Electrical Characteristics**

A. Dodabalapur; L. Torsi; H. E. Katz

Science, New Series, Vol. 268, No. 5208. (Apr. 14, 1995), pp. 270-271.

Stable URL:

http://links.jstor.org/sici?sici=0036-8075%2819950414%293%3A268%3A5208%3C270%3AOTTTAI%3E2.0.CO%3B2-E